Submitted as Short Communication to the *Journal of the European Ceramic Society*, April 2011. Revised in August 2011.

Crystal-Size Dependence of the Spark-Plasma-Sintering Kinetics of ZrB_2 Ultra-High-Temperature Ceramics

V. Zamora [a], A.L. Ortiz [a,*], F. Guiberteau [a], M. Nygren [b]

[a] Departamento de Ingeniería Mecánica, Energética y de los Materiales, Universidad de Extremadura, Badajoz, Spain

[b] Department of Materials and Environmental Chemistry, University of Stockholm, 10691 Stockholm, Sweden

Abstract

The crystal-size dependence of the spark-plasma-sintering (SPS) kinetics of ZrB_2 ultra-high-temperature ceramics (UHTCs) was investigated. It was found that refining the starting powder enhances the SPS kinetics, reducing the onset temperatures of sintering and of the intermediate and final sintering regimes, as well as promoting a greater maximum shrinkage rate at lower temperatures. This enhancement was only relevant with reduction in crystal size to the nanoscale. Finally, the implications for low-temperature sintering of ZrB_2 UHTCs are discussed.

Keywords: ZrB_2; ultra-high-temperature ceramics; spark-plasma sintering; crystal size.

* Corresponding author:
Angel L. Ortiz
Phone: +34 924289600 Ext: 86726
Fax: +34 924289601
E-mail: alortiz@materiales.unex.es

1. Introduction

Ultra-high-temperature ceramics (UHTCs) are a key element for progress in various extreme-environment aerospace applications such as hypersonic flight, scram-jet propulsion, rocket propulsion, and atmospheric re-entry [1]. Zirconium diboride (ZrB_2) is one of the short list of candidate UHTCs, and probably the one that has received most attention to date [2,3]. Unfortunately, one of the major obstacles for the development and implementation of ZrB_2 UHTCs is that the serious kinetic constraints imposed by the combination of the strong covalent bonding, low self-diffusion coefficients, oxygen impurities on the particle surfaces, and large particle sizes makes it impossible to densify the typical commercially available micrometre ZrB_2 powders by conventional sintering (pressureless sintering or hot pressing) at moderate temperatures [2,3]. It is not surprising therefore that the search for a solution to the problem of the poor sinterability of ZrB_2, as also of other UHTCs, is an area of particular interest for research [2,3].

It is well known that the sinterability of highly covalent-bonded ceramics can be enhanced by refining the starting powders due to the reduction in the diffusion distance of chemical species [4]. This is also true for ZrB_2 UHTCs, as has recently been demonstrated by Thompson et al. [5]. They pressureless sintered pure ZrB_2 powders with two crystal sizes under the same conditions, and found that the density increased by ~10% in the temperature range 1600-2100 °C when the crystal size was reduced by attrition milling from the as-purchased condition of ~2 μm down to ~0.2 μm, although the densification was anyway still very limited (i.e., as low as 75% at 2100 °C for the ball-milled powder) [5]. They also observed with the same powders that the relative density reached by spark-plasma sintering at 1900 °C for 5 min increased from ~70 to 97% with crystal size refinement from the micrometre to the submicrometre range [5]. These and other observations [2,3,5,6] have reinforced the commonly held belief that ZrB_2 is intrinsically unsinterable without pressure in the pure state, but that it can be densified by spark-plasma sintering (SPS) or hot pressing at nearly 1900 °C if the starting powders are refined appropriately, because the sintering kinetics of pure ZrB_2 depends on crystal size. However, investigation into the crystal-size dependence of the sintering kinetics of pure ZrB_2 UHTCs has been limited to studying the densification data corresponding to micrometre or submicrometre crystal sizes. No information exists for crystals at the nanoscale, even though this is the scale at which one expects improvement in the kinetic performance of the powder to be most relevant. This underscores the need to include more crystal sizes in a systematic densification study of pure ZrB_2 UHTCs in order to determine

the broader trend of the crystal size dependence of ZrB_2 density. The present study was therefore aimed at comparing the SPS kinetics of micrometre, submicrometre, and nanocrystalline ZrB_2 powders without additives. Although SPS is similar to HP in that they both apply a uniaxial load, it has the advantage that the pulsed electrical current heats the die (and the compact if the powder is electrically conductive) directly, and the rapid sintering cycles enable better control of the final microstructure and therefore of the properties of the resulting material [7-10]. Since the fine and ultra-fine ZrB_2 powders are typically prepared by milling the commercially-available coarse powders, the broader objective of the present study is to advance towards the lower-temperature sintering of ZrB_2 UHTCs via the optimization of the comminution practice.

2. Experimental procedure

A commercially available micrometre powder of ZrB_2 (Grade B, H.C. Starck) was chosen as starting material to prepare the rest of the powders. To this end, the as-purchased powder of single-crystal particles of 2 μm average size was subjected to high-energy ball-milling in a shaker miller (Spex D8000, Spex CertiPrep) operated at about 1060 back-and-forth cycles per minute. The milling was carried out in cylindrical hardened-steel containers with WC balls (6.7 mm in diameter) under a ball-to-powder weight ratio of 4, and for times in the range 1–180 min to impart different degrees of milling intensity to the as-purchased ZrB_2 powder, and thus create an ample set of ZrB_2 powders with crystal sizes ranging progressively from ~2 μm all the way down to just some nanometres (in particular, 10 nm). The X-ray diffractometry (XRD; D8 Advance, Brukers AXS) analysis[a] of the ball-milled powders shown in Fig. 1 revealed that there indeed occurred such a progressive decrease in crystal size with increasing high-energy ball-milling time, but the laser-scatting analysis (LS; Mastersizer 2000, Malvern Instruments) of the powders shown in Fig. 2 indicated that the nano-crystals achieved with the long-time high-energy ball-milling had actually agglomerated [11,12]. The LS analysis also indicated that the particle size distributions were all unimodal, and with similar relative size dispersion (i.e., ~1.5-1.7 as measured in term of $(D_{90}\text{-}D_{10})/D_{50}$).

[a] To allow the valid measurement of the crystal size in all ball-milled powders, the XRD data of the most intense peak of ZrB_2 (i.e., its 101 peak) were collected using a high-resolution diffractometer equipped with a primary monochromator that provides pure $CuK\alpha_1$ radiation as well as with an ultra-fast linear detector, and configured with thin slits to ensure a very sharp instrumental broadening, and the calculations were made by applying the variance method with Voigt profile functions [13]. Furthermore, the crystal sizes so-calculated have been validated by transmission electron microscopy elsewhere [11].

The different ZrB_2 powders were individually loaded into a 12-mm diameter graphite dies lined with graphite foil, and were spark-plasma sintered (Dr. Sinter SPS-2050, Sumitomo Coal Mining Co.) in dynamic vacuum (i.e., ~6 Pa) up to 1900 °C. The temperature was first raised to 600 °C in 3 min, and thence onwards was measured by an optical pyrometer focused on the die. The heating ramp was set at 200 °C·min^{-1} up to 1200 °C, and at only 100 °C·min^{-1} from 1200 to 1900 °C because, this being the critical densification range [14], it was advisable to monitor the progress in more detail. A uniaxial pressure of 50 MPa was applied up to 1200 °C, and was then increased to 75 MPa and maintained until completion of the sintering cycle. The soaking at 1900 °C lasted as long as was required for the punches to cease traveling, at which moment the load was released and the electrical power was shut off to allow rapid cooling to room temperature (i.e., in 1-2 min). The SPS furnace is equipped with a dilatometer of resolution better than 0.001 mm, connected to a computer to log the shrinkage curves. These curves were corrected for the expansion of the graphite parts (i.e., die, punches, and spacers) to give the real shrinkage curve of the powder itself. The densification curves were reconstructed from the shrinkage curves by considering the relative densities of the sintered samples. These relative densities were determined by first measuring the absolute density by the Archimedes method using distilled water as the immersion medium, and then dividing by the density of the powder measured by helium pycnometry (Multipycnometer, Quantachrome Instruments). The microstructure of the sintered materials was observed by scanning electron microscopy (S-3600N, Hitachi) to validate the porosity data.

3. Results and discussion

Figure 3 shows the densification curves as a function of time for the ZrB_2 powder before and after the different degrees of milling intensity. It can be seen that the curves all have the same general shape, i.e., there is first a plateau, then the sintering progresses moderately, then much more abruptly, and lastly gradually towards the ultimate densification. It can also be seen in Fig. 3 that with increasing ball-milling time the densification curves shift towards lower times, i.e., towards lower temperatures, and that the ultimate densification increases. Both these aspects constitute clear evidence that the high-energy ball-milling enhances the sintering kinetics of ZrB_2. Note that the improvement in kinetic performance of the powder cannot be attributed to possible contamination by WC that would help in the densification because (i) this was only detected in a minimal amount (i.e., less than 2.5 wt% of WC as measured by XRD through the Rietveld method

and confirmed by energy-dispersion X-ray spectroscopy) in the powder with 180 min of ball-milling [15] while the enhancement in sintering behaviour is observed for all ball-milled powders, and (ii) the thermodynamic calculation shows that the removal reaction of ZrO_2 by WC is favorable above 1944 °C [16], and indeed WC has been observed to act as a pressureless sintering additive above 2100 °C [17]. Three different forms of sintering behaviour can be distinguished in Fig. 3. Firstly, there is the as-purchased powder with a micrometre crystal size of ~2 μm, which has the slowest sintering kinetics; secondly there are the powders ball-milled for 1, 3, and 5 min which have somewhat faster sintering kinetics than that of the as-purchased powder; and thirdly, there are the powders ball-milled for 30, 60, and 180 min which have much faster sintering kinetics than the rest of the powders. The kinetics of the powder ball-milled for 10 min is intermediate between that of the powders with short (1, 3, and 5 min) and long (30, 60, and 180 min) ball-milling times. According to Fig. 1, it can be concluded that the kinetics improvement is only moderate when the crystal size is refined to within the submicrometre range (i.e., ball-milling times of 1, 3, and 5 min), but notable when the crystal size is refined to within the nanoscale (i.e., ball-milling times of 30, 60, and 180 min). These results have important practical implications because they reveal that high-energy ball-milling can provide ZrB_2 powders with the superior kinetic performance not achievable today via attrition milling. Note that attrition milling has been so far the gold standard comminution treatment of ZrB_2 powders, but it refines the crystal sizes only down to ~0.5-0.2 μm, a size scale at which improvement in sintering behaviour was found to be only moderate (see Fig. 3).

Let us now examine the densification curves in greater detail. Firstly, it can be seen in Fig. 3 that the initial densification (henceforth termed green-body densification because the density measurements performed on selected powders showed no differences in the degree of densification at 25 °C and at the onset of the SPS cycle at 600 °C) has a complex dependence on ball-milling time, and does not correlate with the crystal size since as it first increases, then decreases, and finally again increases slightly or stabilizes within the errors despite the crystal size decreasing progressively with ball-milling time (see Fig. 1). This observation was not a surprise because the powder packing density scales inversely with powder particle sizes [18], not with crystal sizes. As shown in Fig. 2, the evolution of the green-body densification with ball-milling time follows qualitatively the inverse trend of the average powder particle size. This simplistic correlation between the green-body densification and the average powder particle size is probably because the

particle size distributions are all unimodal and self-similar. Secondly, it can also be seen in Fig. 3 that the densification curves all exhibit a densification jump at ~260-265 s (i.e., at 850-880 °C), followed by a gradual linear increase in densification. This jump and the subsequent linear stretch of densification can be attributed to mechanical compaction of the powder [19]. A second densification jump is also observed at ~370-380 s (i.e., at ~1200 °C), which is when the load was increased from 50 to 75 MPa. Thirdly, the temperature for the onset of sintering (T_{OS}), which is the temperature at which the curves start to deviate from the linear compaction stretch, decreases continuously with decreasing crystal size. In particular, as shown in Fig. 4 the decrease in T_{OS} is only moderate with the reduction of crystal size within the submicrometre range (to ~100 nm), but abrupt from there on downwards. This same trend is also apparent for the temperature of the onset of the intermediate stage of sintering (T_{OIS}), which is the sintering regime in which the open porosity is eliminated and typically begins at a relative density of ~70% [20]. The temperature for the onset of the final stage of sintering (T_{OFS}), which is the sintering regime in which the closed porosity is eliminated and typically begins at a relative density of ~90% [20], also drops with reduction in crystal size. Thus, whereas in the as-purchased powder and in the powders ball-milled for 1, 3, and 5 min the final stage of sintering initiates after the isothermal heating at 1900 °C for 272, 42, 35, and 25 s, respectively, it occurs in the non-isothermal regime at 1900 °C in the powder ball-milled for 10 min and at 1770±10 °C in the powders with 30, 60, and 180 min of ball-milling. And fourthly, the degree of non-isothermal densification and the ultimate densification also improve with the reduction in crystal size. Note that the as-purchased powder with micrometre-sized crystals reached only ~78% density at 1900 °C, which increased up to ~96% after the isothermal heating at 1900 °C for 13 min. The powders with submicrometre-sized crystals (i.e., those ball-milled for 1, 3, and 5 min) reached a greater density of ~86-88% at 1900 °C, and almost full density (>98%) when soaked there for ~6 min. The ultra-fine powder ball-milled for 10 min densified up to ~91% at 1900 °C, and up to ~99% when maintained at 1900 °C for 6 min. Finally, the nano-powders (i.e., those ball-milled for 30, 60, and 180 min) reached ~98% density at 1900 °C, and densified completely after a brief soaking time at 1900 °C that was indeed shorter with decreasing crystal size (i.e., 228, 150, and 144 s, for the 26, 17, and 9 nm sizes, respectively). The direct observation of the microstructures by SEM confirmed these densification data. As shown in Fig. 5a-b, pores can be clearly seen in the UHTC fabricated from the as-purchased powders, whereas they were hardly discernible in the rest of the UHTCs. It is also observed in the SEM

micrographs that the UHTCs fabricated from the ball-milled powders contain small particles located at grain boundaries and multigrain junctions. These were identified as being ZrO_2 by energy-dispersive X-ray analysis (see Fig. 5c), and confirmed by XRD (not shown). The formation of ZrO_2 is consistent with the fact that the high-energy ball-milling was conducted in air, and therefore there is oxygen uptake on the crystal surfaces – from 1.537 wt% in the as-purchased condition to 4.514 wt% after 180 min of high-energy ball-milling, as measured by the inert gas (helium) fusion method. Since these oxide impurities are known to favour coarsening over densification [2,3,17,21,22], it is reasonable to think that the kinetic effect of the crystal size reduction is more pronounced than observed here. Indeed, that the oxidation uptake hinders densification can be seen clearly in Fig. 3 on comparing the last stretches in the densification curves of the powders ball-milled for 60 and 180 min. Finally, also evident comparing Fig. 5a and b is that the grains are smaller with decreasing crystal size in the starting powder, although all the sintered UHTCs have micrometre-sized grains because the nanostructure of the ball-milled powders is not retained when sintering at 1900 °C.

Figure 6 shows the maximum shrinkage rate (V_{MSR}) and the temperature at which this is reached (T_{MSR}), as determined from the time derivative of the shrinkage curves. The analysis of these data is also very interesting. It can be seen that V_{MSR} increases continuously with decreasing crystal size. However, the increase is first moderate from ~5 μm·s^{-1} up to ~6.4 μm·s^{-1} with reduction in crystal size from 2 μm down to 0.5 μm, and then there is a slight rise up to ~7 μm·s^{-1} as the crystal size is refined down to 100 nm, followed by an abrupt rise up to ~12 μm·s^{-1} as the crystal size decreases to 10 nm. It can be also seen in the figure that T_{MSR} decreases continuously with decreasing crystal size. In particular, the fall in T_{MSR} is only marginal from ~1810 to ~1750 °C as the crystal size decreases to 100 nm, but then falls abruptly to ~1550 °C as the crystal size is reduced to 10 nm. In solid-state sintered materials as in the present case, the maximum in the densification-rate curve is attributed to the change in the mechanism responsible for mass transport from surface diffusion to grain-boundary diffusion [23]. Surface diffusion produces neck growth and grain coarsening, but does not cause significant densification [20]. Grain-boundary diffusion, on the contrary, produces marked densification [20]. It can thus be concluded that the high-energy ball-milling promotes greater grain-boundary diffusion in ZrB_2 at lower temperatures. This can be understood by considering that high-energy ball-milling refines the crystal sizes (see Fig. 1), shortening the diffusion distances of the Zr and B species and inducing the formation of a greater

density of grain boundaries available as faster diffusion paths, and also activates them mechanically by introducing surface defects that also increase the diffusion coefficient [24]. Indeed, the temperature reduction with decreasing crystal size is an established fact in the framework of solid-state sintering theory [20]. Consider a powder with crystals of size D_1 that reaches a given degree of densification at temperature T_1. It has been demonstrated that with the change in crystal size from D_1 to D_2 this powder will reach the same degree of densification at a temperature T_2 given by the expression [20]:

$$T_2 = \frac{1}{\frac{1}{T_1} - \frac{km}{Q} ln \frac{D_2}{D_1}}$$

where *k* is Boltzmann's constant, *m* is a constant that depends on the mass transport mechanism, and *Q* is the activation energy. If D_2 is less than D_1 then a reduction in the sintering temperature is predicted (i.e., $T_2 < T_1$). This is indeed the trend observed experimentally. Unfortunately, the activation energy of the grain-boundary diffusion in ZrB_2, responsible for its densification, cannot be inferred from the data of T_{OIS}, T_{MSR}, or T_{OFS} because T_{OIS} is reached in the sintering regime controlled by surface diffusion, T_{MSR} is reached at different degrees of densification, and T_{OFS} is reached in many cases during the regime of isothermal heating at 1900 °C. To compute this activation energy, the temperature at which 80% of densification is achieved ($T_{80\%}$) was measured, and is also plotted in Fig. 4. The choice of $T_{80\%}$ is because, with the degree of densification being a constant, it falls within the regime of non-isothermal heating controlled by grain-boundary diffusion for all the powders except the as-purchased powder which will not be included in the calculations. Applying the above expression with *m*=4 for grain-boundary diffusion, the activation energy is found to be 1600 kJ/mol. This is a very high activation energy, which explains why the commercially-available ZrB_2 powders with micrometre-sized particles are considered to be intrinsically unsinterable without sintering additives at moderate temperatures.

Finally, it is worthwhile to discuss briefly the relevance and potential implications derived from the results and discussion. The present study reveals that crystal size refinement enhances the SPS kinetics of ZrB_2 powders, and most likely that of pressureless sintering and hot-pressing, but that the enhancement is relevant only with reduction in crystal size down to the nanoscale. This underscores the importance of using high-energy ball-milling for the preparation of the ZrB_2

starting powders, since the nanoscale is not really achievable by conventional attrition milling. Furthermore, the shrinkage rate data are especially interesting because they suggest that it would in principle be possible to densify ZrB_2 UHTCs with minimal grain coarsening close to the temperature dictated by T_{MSR} as a function of the crystal size, if these powders were sufficiently isothermally soaked at such a temperature under the appropriate compaction pressure. One could then process ZrB_2 UHTCs both at lower temperatures than required today and with finer microstructures, both of which aspects are objectives being intensively pursued by the ceramics community. Elucidation of this expectation, however, requires further sintering studies on ZrB_2.

4. Conclusions

A commercially-available micrometer ZrB_2 powder was subjected to different degrees of high-energy ball-milling intensity to investigate the crystal-size dependence of the SPS kinetics of ZrB_2 UHTCs within the micrometre, submicrometre, and nanometer ranges. The following conclusions can be drawn:

1. The crystal size refinement enhances the SPS kinetics of ZrB_2 powders, reducing the onset temperatures of sintering and of the intermediate and final sintering regimes, as well as promoting a greater maximum shrinkage rate at lower temperatures.
2. The enhancement in the kinetic performance of the powder is moderate with the reduction of the crystal size within the submicrometre range, but relevant with the refinement down to the nanoscale.
3. The activation energy for grain-boundary diffusion in ZrB_2 is 1600 kJ/mol, which is very high and accounts for the unsinterability of the coarse ZrB_2 powders without sintering additives at moderate temperatures.
4. High-energy ball-milling can provide the ZrB_2 starting powders with the kinetics performance not achievable today by conventional attrition milling. It may therefore have an important role to play in the lower-temperature sintering of ZrB_2 UHTCs.

Acknowledgements. This work was supported by the Ministerio de Ciencia y Tecnología (Government of Spain) under Grant N° MAT 2007-61609.

References

1. Wuchina E, Opila E, Opeka M, Fahrenholtz W, Talmy I. UHTCs: Ultra-High Temperature Ceramic Materials for Extreme Environment Applications. *Interface* 2007;**16**(4) 30–36.
2. Fahrenholtz WG, Hilmas GE, Talmy IG, Zaykoski JA. Refractory Diborides of Zirconium and Hafnium. *J Am Ceram Soc* 2007; **90**(5):1347–64. See also references therein.
3. Guo S-Q. Densification of ZrB_2-Based Composites and their Mechanical and Physical Properties: A Review. *J Eur Ceram Soc.* 2009;**29**(6):995–1011. See also references therein.
4. Rahaman MN. Ceramic Processing and Sintering. Marc el Dekker, New York; 1995.

5. Thompson M, Fahrenholtz WG, Hilmas G. Effect of Starting Particle Size and Oxygen Content on Densification of ZrB_2. *J Am Ceram Soc.* 2011;**94**(2):429–35.
6. Bellosi A, Monteverde F, Sciti D. Fast Densification of Ultra-High-Temperature Ceramics by Spark Plasma Sintering. *Int. J. Appl. Ceram. Technol*. 2006;**3**(1) 32–40.
7. Nygren M, Shen Z. Spark Plasma Sintering: Possibilities and Limitations. *Key Eng Mater*. 2004;**264-268**:719–24.
8. Munir ZA, Anselmi-Tamburini U, Ohyanagi M. The Effect of Electric Field and Pressure on the Synthesis and Consolidation of Materials: a Review of the Spark Plasma Sintering Method. *J Mat Sci*. 2006;**41**(3):763–77.
9. Munir ZA, Quach DV, Ohyanagi M. Electric Current Activation of Sintering: a Review of the Pulsed Electric Current Sintering Process. *J Am Ceram Soc.* 2011;**94**(1):1–19.
10. Orru R, Licheri R, Locci AM, Cincotti A, Cao G. Consolidation/Synthesis of Materials by Electric Current Activated/Assisted Sintering. *Mat Sci Eng R*. 2009;**63**(4-6):127–287.
11. Galán CA, Ortiz AL, Guiberteau F, Shaw LL. Crystallite Size Refinement of ZrB_2 by High-Energy Ball Milling. *J Am Ceram Soc.* 2009;**92**(12):3114–7.
12. Galán CA, Ortiz AL, Guiberteau F, Shaw LL. High-Energy Ball Milling of ZrB_2 in the Presence of Graphite. *J Am Ceram Soc.* 2010;**93**(10):3072–5.
13. Sánchez-Bajo F, Ortiz AL, Cumbrera FL. Analytical formulation of the variance method of line-broadening analysis for voigtian X-ray diffraction peaks. *J Appl Crystallogr*. 2006;**39**(4):598–600.
14. Guo S-Q, Nishimura T, Kagawa Y, Yang J-M. Spark Plasma Sintering of Zirconium Diborides. *J Am Ceram Soc.* 2008;**91**(9):2848–55.
15. Zamora V, Ortiz AL, Guiberteau F, Shaw LL, Nygren M. On the Crystallite Size Refinement of ZrB_2 by High-Energy Ball-Milling in the Presence of SiC. *J Eur Ceram Soc.* 2011;**31**(13):2407–14.
16. Fahrenholtz WG, Hilmas GE, Zhang SC, Zhu S. Pressureless Sintering of Zirconium Diboride: Particle Size and Additive Effects. *J Am Ceram Soc.* 2008;**91**(5):1398–1404.
17. Chamberlain AL, Fahrenholtz WG, Hilmas GE. Pressureless Sintering of Zirconium Diboride. *J Am Ceram Soc.* 2006;**89**(2):450–6.
18. German RM. Powder Metallurgy Science. Metal Powder Industries Federation, Princeton, NJ; 1994.

19. Silvestroni L, Bellosi A, Melandri C, Sciti D, Liu JX, Zhang GJ. Microstructure and Properties of HfC and TaC-based Ceramics Obtained by Ultrafine powder. *J Eur Ceram Soc.* 2011;**31**(4):619–27.
20. German RM. Sintering Theory and Practice. Wiley, New York; 1996.
21. Dole SL, Prochazka S, Doremus RH. Microstructural Coarsening during Sintering of Boron Carbide. *J Am Ceram Soc.* 1989;**72**(6):958–66.
22. Zhang SC, Hilmas GE, Fahrenholtz WG. Pressureless Densification of Zirconium Diboride with Boron Carbide Additions. *J Am Ceram Soc.* 2006;**89**(5):1544–50.
23. Shen Z, Nygren M. Microstructural Prototyping of Ceramics by Kinetic Engineering: Applications of Spark Plasma Sintering. *Chem Rec* 2005;**5**(3):173–84.
24. Suryanarayana C. Mechanical Alloying and Milling. *Prog Mater Sci*. 2001;**46**(1-2):1–184.

Figure Captions

Figure 1. Average size of the ZrB_2 crystals as a function of high-energy ball-milling time, determined by XRD. The points are the experimental data, and the solid line is merely to guide the eye. The crystal size in the as-purchased condition was taken to be the same as the particle size measured by electron microscopy.

Figure 2. Average particle size in the ZrB_2 powders as a function of high-energy ball-milling time, determined by LS. Also included is the green-body densification for the ZrB_2 without and with the

high-energy ball-milling. The points are the experimental data, and the solid lines are merely to guide the eye.

Figure 3. SPS-densification curves as a function of time for the as-purchased ZrB_2 powder and the ZrB_2 powders subjected to high-energy ball-milling. The points are the experimental data. The solid line indicates the temperature profile used. The dashed line separates the regimes of non-isothermal and isothermal heating during the SPS cycle.

Figure 4. Evolution of T_{OS} T_{OIS}, and $T_{80\%}$ with the reduction in crystal size. The points are the experimental data, and the solid lines through the T_{OS} and T_{OIS}data are merely to guide the eye. The thicker solid line through the $T_{80\%}$ data is the fit used to compute the activation energy of the grain-boundary diffusion in ZrB_2. The dashed line is the prediction of the fit for the crystal size of the as-purchased powder. The open and semi-closed triangles are the values of $T_{80\%}$ determined for the as-purchased powder in the isothermal heating regime and the extrapolation of the non-isothermal densification curve to 80% of relative density, respectively.

Figure 5. SEM micrographs of the ZrB_2 UHTCs processed from the (a) as-purchased powder and (b) the powder with 180 min of high-energy ball-milling. (c) Energy-dispersive X-ray spectra taken in spot mode on the grains and small particles in the SEM micrograph of Fig. 5b.

Figure 6. Evolution of V_{MSR} and of T_{MSR} with the reduction in crystal size. The points are the experimental data, and the solid lines are merely to guide the eye.

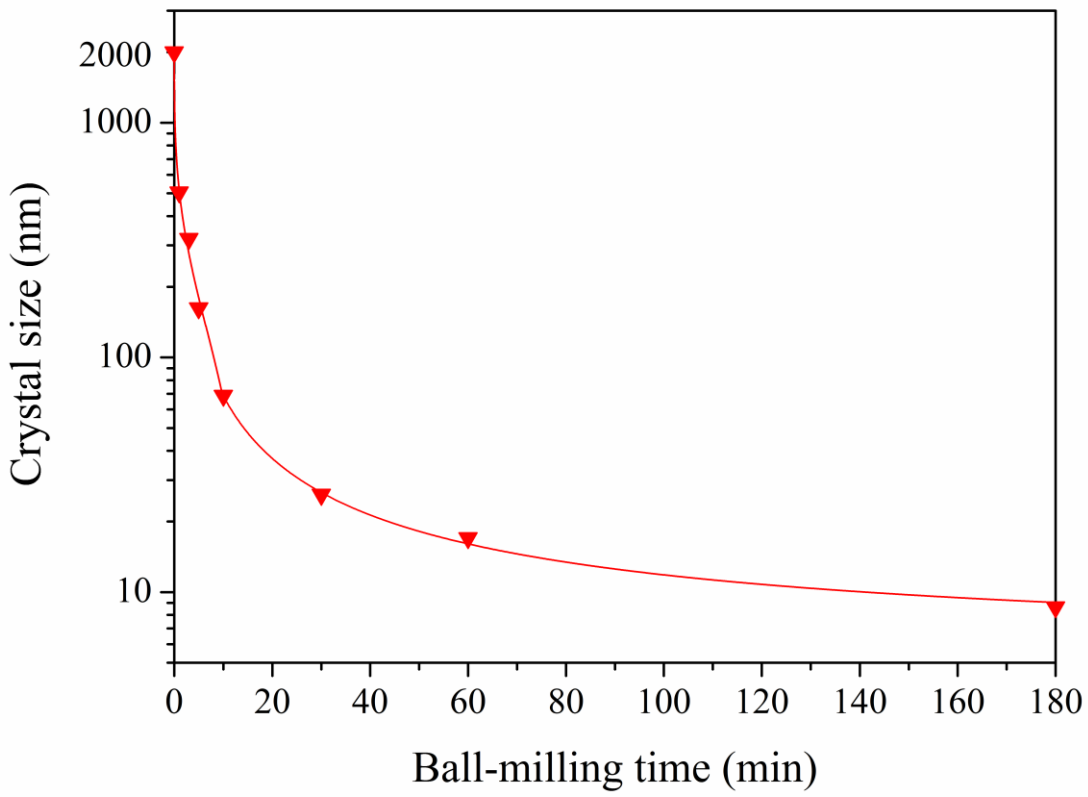

V. Zamora *et al.*
Figure 1

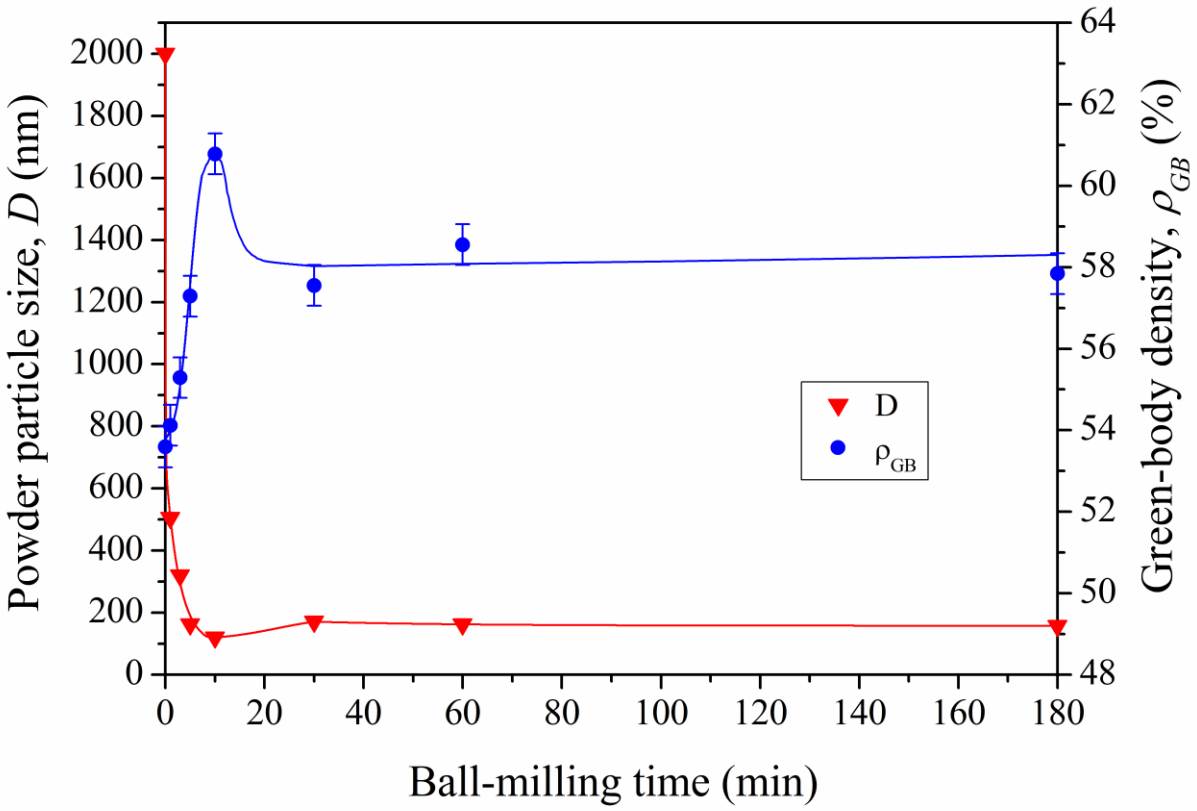

V. Zamora *et al.*
Figure 2

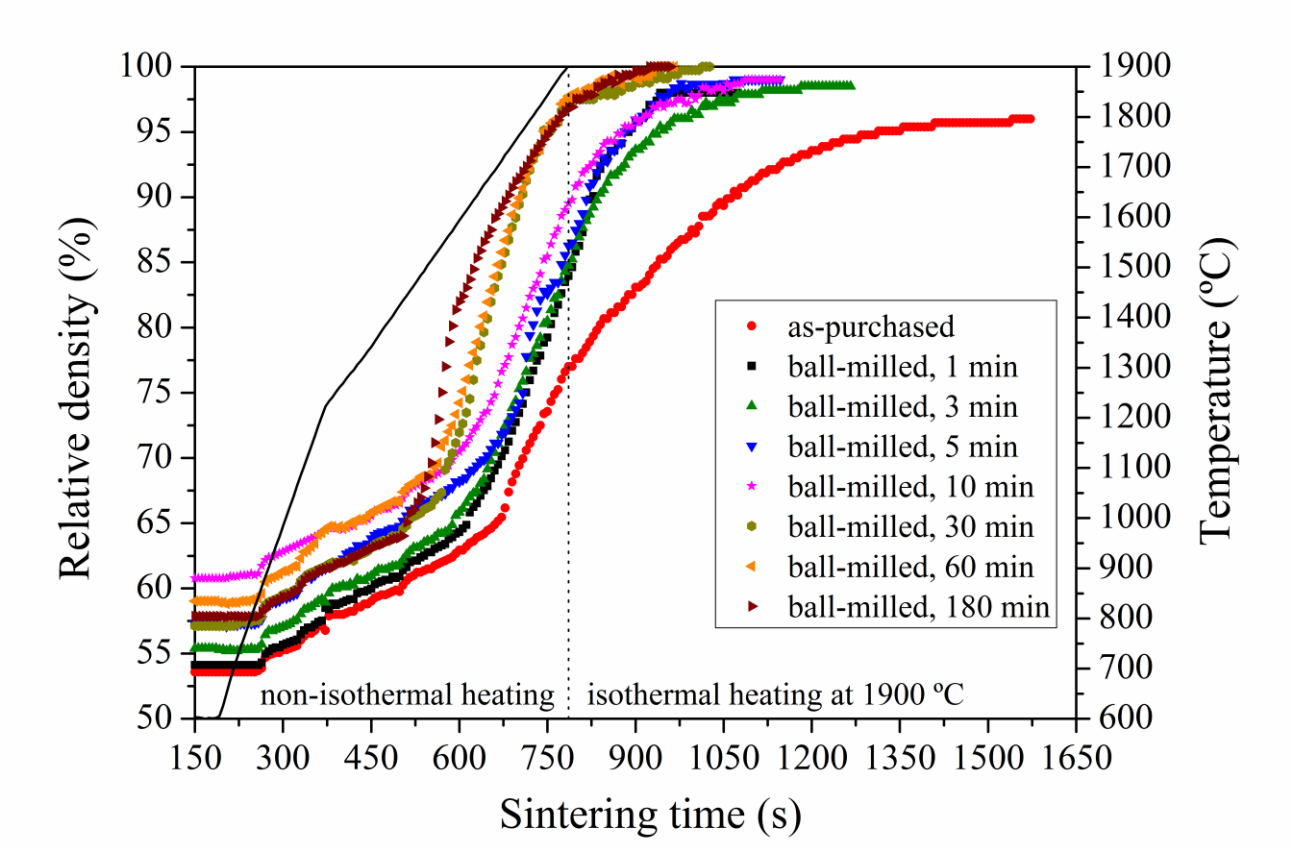

V. Zamora *et al.*
Figure 3

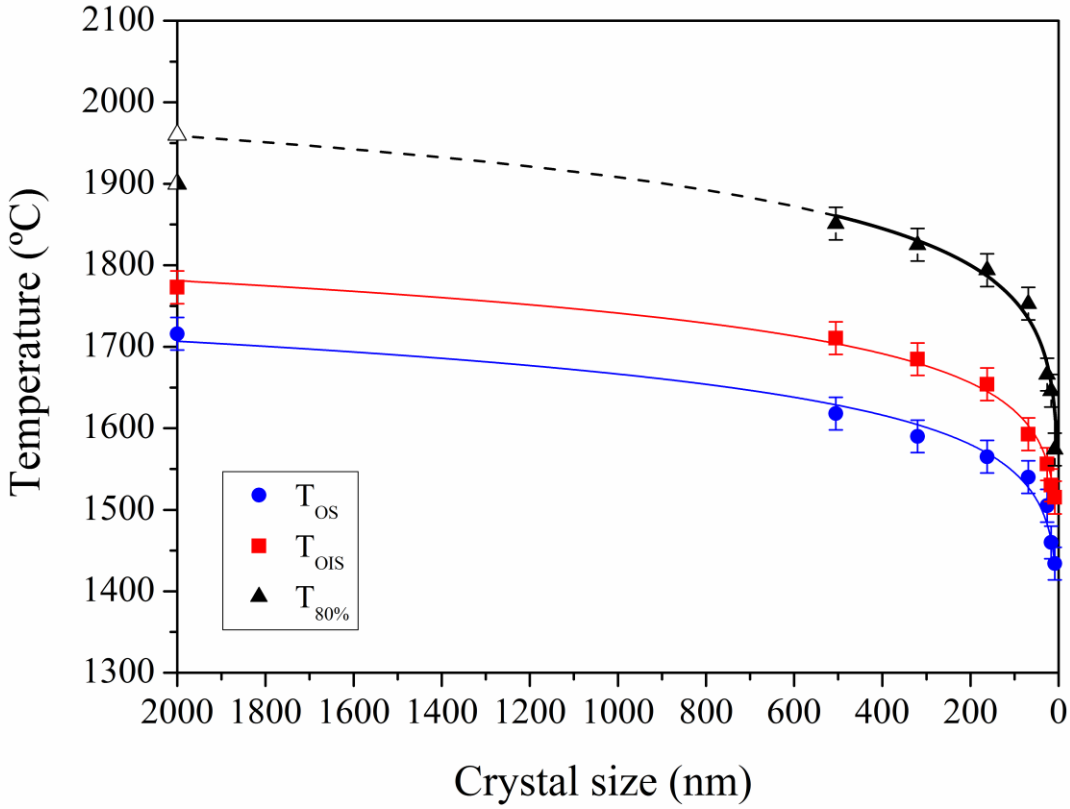

V. Zamora *et al.*
Figure 4

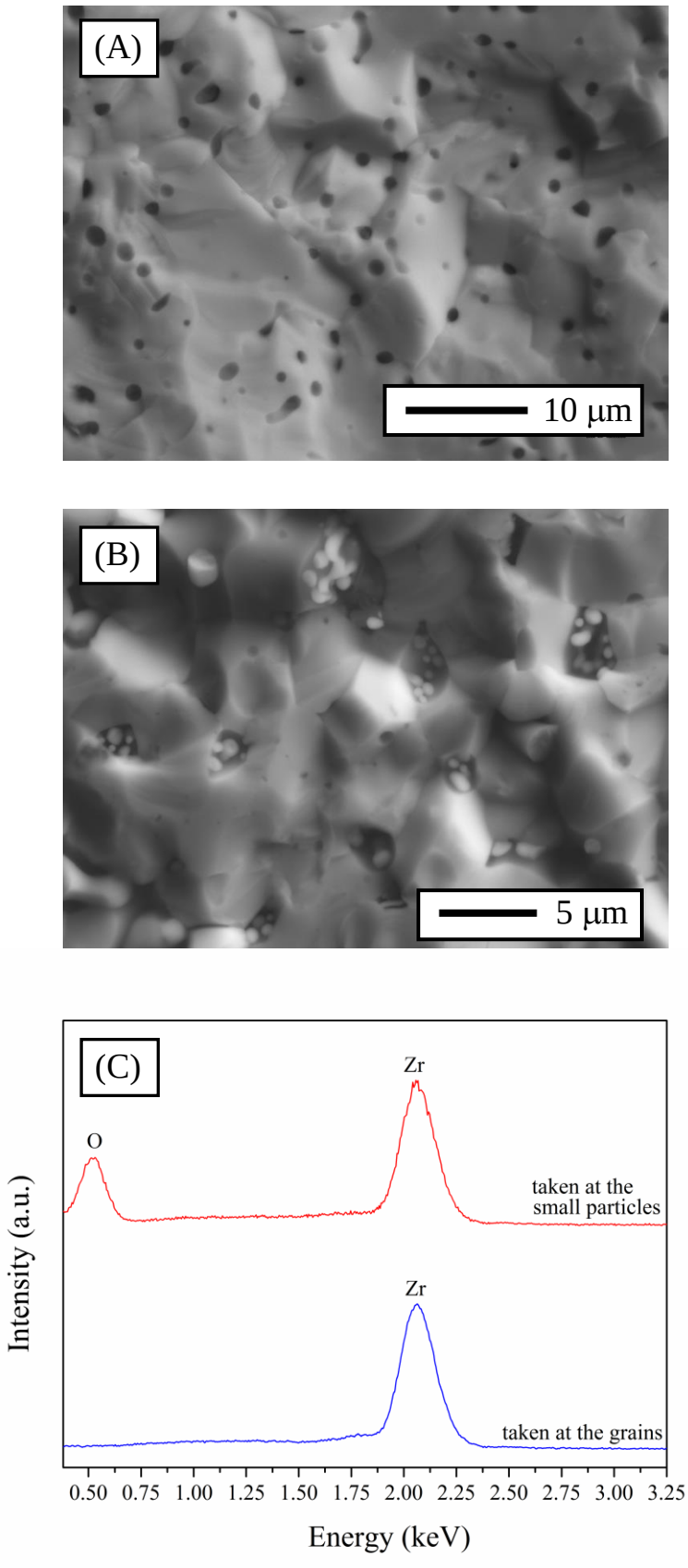

V. Zamora *et al.*
Figure 5

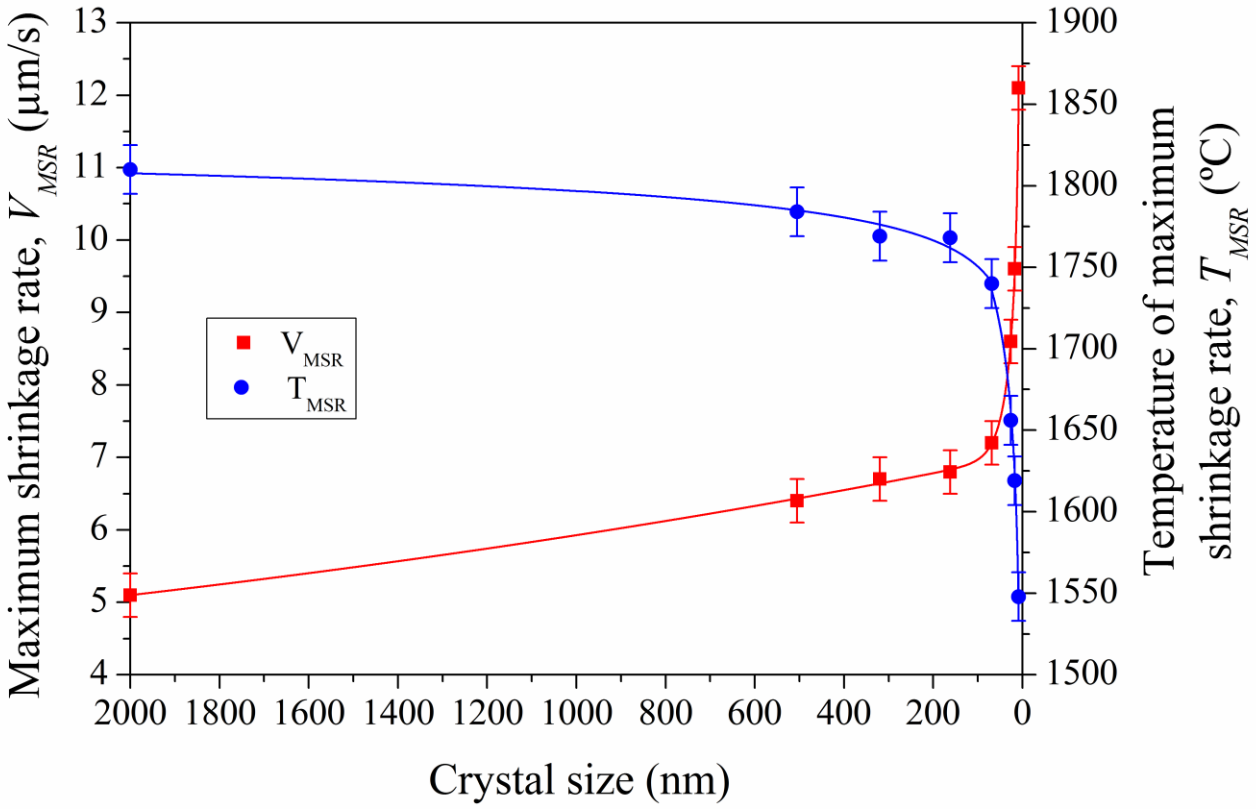

V. Zamora *et al.*
Figure 6